

Research Article

Tobias Kehrer and Samuel Arba Mosquera*

A simple cornea deformation model

<https://doi.org/10.1515/aot-2021-0039>

Received August 18, 2021; accepted October 29, 2021;
published online November 26, 2021

Abstract: In this paper, we present a cornea deformation model based on the idea of extending the ‘neutral axis’ model to two-dimensional deformations. Considering this simple model, assuming the corneal tissue to behave like a continuous, isotropic and non-compressible material, we are able to partially describe, e.g., the observed deviation in refractive power after lenticule extraction treatments. The model provides many input parameters of the patient and the treatment itself, leading to an individual compensation ansatz for different setups. The model is analyzed for a reasonable range of various parameters. A semi-quantitative comparison to real patient data is performed.

Keywords: biomechanics; computer simulation; laser vision correction.

1 Introduction

A modern refractive surgery treatment is the small incision lenticule extraction (SMILE) by VisuMAX (Carl Zeiss Meditec, Jena, Germany) [1, 2] as well as SmartSight by SCHWIND ATOS (SCHWIND eye-tech-solutions, Kleinostheim, Germany) [3–6] and CLEAR by Femto LDV Z8 (Ziemer Ophthalmics, Port, Switzerland) [7–9]. All of these treatments are based on the change of refractive power of the cornea due to a lenticule extraction and provide several advantages compared to laser assisted *in situ* keratomileusis (LASIK) and photorefractive keratectomy (PRK). The cuts inside the cornea are performed by a near infrared femtosecond laser. The surgery is conducted while the cornea/eye is docked to a patient interface (PI), which isolates the cornea/eye from the laser system, also electrically. It furthermore neutralizes the refractive power of the eye due to a suitable choice of the refractive index of the PI

material. Since the cornea/eye is docked, the anterior surface of the cornea is therefore defined and fixed during treatment.

Within [6, 10–12], a postoperative undercorrection of approximately 9–16% with respect to the planned correction is observed. This motivates the search for future treatment improvements.

In this paper, we will focus on the influence of the docking to the PI on various treatment parameters, e.g., refractive power change. The aim is to find a mathematically easy model to describe the deformation behavior of the cornea up to a certain level. We will especially focus on transformations like the docking of the eye to the PI but also the closing of the lenticule. Rather complex mathematical/computational models are, e.g., elaborated in [13–19], which make use of FEM methods that can respect some microscopic fiber/anisotropic structure of the corneal tissue. Furthermore, a whole issue was dedicated to ‘Corneal Biomechanics’ [20]. Other models and estimations of output parameters by input parameters are, e.g., illustrated in [10, 12, 21]. The initial starting point of our rather macroscopic model follows the idea of the ‘neutral axis’, cf. Euler-Bernoulli beam theory or later extended to Timoshenko-Ehrenfest beam theory [22]. If the considered transformation of a material can be viewed as a one-dimensional deformation, e.g., 1D bending of a beam, the principle of the ‘neutral axis’ might be applied. This axis represents the set of points inside the material that do not experience stretching or compression. Therefore, its length remains unchanged under deformation of the material. A schematic visualization is presented in Appendix A. For a two-dimensional deformation, like the docking of the cornea to the PI, a different principle has to be employed. The naive ansatz is to directly translate the principle ‘neutral axis’ to two dimensions. Whereas when the length of the ‘neutral axis’ is conserved, the ‘neutral membrane’ experiences a conserved area. A schematic visualization of a radial slice of the cornea under a two-dimensional deformation is given in Appendix A. In reality, the movement/stretching of the corneal tissue is limited. Effectively, at some distance from the vertex the cornea is fixed, e.g., at limbus. Therefore, a modification of the initial scheme has to be developed.

This paper is structured as follows. In Section 2, the basics of the model considering the fixation of the cornea at some distance from the vertex are presented. Consequently, its mathematical description is formulated. In Section 3, the

*Corresponding author: Samuel Arba Mosquera, SCHWIND Eye-Tech-Solutions GmbH, Mainparkstrasse 6-10, D-63801 Kleinostheim, Germany, E-mail: samuel.arba.mosquera@eye-tech.net
<https://orcid.org/0000-0002-3152-0557>

Tobias Kehrer, SCHWIND eye-tech-solutions GmbH, Mainparkstraße 6-10, D-63801 Kleinostheim, Germany,
E-mail: tobias.kehrer@protonmail.com. <https://orcid.org/0000-0002-2500-8864>

results obtained via a list of different scenarios of a variety of input parameters are provided and later on discussed in Section 4. In Section 5, we want to give an estimation of future use of this model. The Appendices A, B, and C provide further details on the methods and the findings, whereas the interpretation of the most relevant findings is incorporated into the main body of this work.

2 Deformation model

The initial schematics of the deformation are describing a free cornea. In reality, however, the docking of the cornea to the PI is realized with a complete eye not the corneal tissue only. Therefore, a fixation of the movement/stretching of the cornea is realized at some distance from the vertex, e.g., at limbus. In our model, this will be implemented by a rescaling of the endpoints of the cornea back to the initial distance from the vertex.

We start by introducing our terminology and coordinates used within this paper to describe the mathematics of the deformation model. Most of the time, we will present 2D slices of the cornea rather than 3D plots. This is possible due to the rotational symmetry that a non-astigmatic cornea experiences,¹ on which we restrict our analysis. In 3D, we define its coordinate system as $(\vec{e}_{r_x}, \vec{e}_\phi, \vec{e}_z)$ (cf. Appendix A), whereas we drop the angular direction in the definition of our two-dimensional coordinate system $(\vec{e}_{r_x}, \vec{e}_z)$. The z -axis is defined to be parallel to the optical axis of the eye, whereas r_x is defined as the radius in the x - y -plane with origin at this optical axis. The vertex (in our model the center of the anterior surface of the cornea) is located at a height $z = 0$ mm and at ‘radial distance’ $r_x = 0$ mm. Since we are working in a 2D coordinate system, a profile p can be simply parametrized by defining its height $z_p(r_x, \phi)$, whereas for rotational symmetric profiles, $z_p(r_x)$ is sufficient. In 3D, the parametrization vector \vec{x}_p is given by

$$\begin{aligned} \vec{x}_p(r_x, \phi) &= \begin{pmatrix} r_x \cos(\phi) \\ r_x \sin(\phi) \\ z_p(r_x) \end{pmatrix} \\ &= R_z(\phi) \begin{pmatrix} r_x \\ 0 \\ z_p(r_x) \end{pmatrix}, \quad 0 < r_x, \quad 0 \leq \phi < 2\pi, \end{aligned} \quad (2.1)$$

which can be interpreted as a rotation around the z -axis (obtained by $R_z(\phi)$) of a 2D vector consisting of an r_x - and z -component, $(r_x, z_p(r_x))$. We assume all relevant profiles p to follow a paraboloid with height

$$z_p(r_x) = z_{0,p} - \frac{r_x^2}{2r_p}. \quad (2.2)$$

This parametrization can be mapped approximately to the one of a spherical profile via their curvature radius r_p

$$z_p(r_x) = z_{0,p} + \sqrt{r_p^2 - r_x^2} - r_p = z_{0,p} - \frac{r_x^2}{2r_p} + \mathcal{O}(r_x^4). \quad (2.3)$$

In Table 1, we present a list of various parameters that will appear in our model.

In order to provide a better overview, this list is given already at this point. The parameters, r_{ca} , r_{cp} , r_{cap} and r_{lent} , are the curvature radii of the various profiles related to the cornea, whereas r_{PI} is the curvature radius of the PI. The central thickness of the cornea (at vertex) is denoted by d_{cc} and the central thickness of the cap and lenticule by d_{ccap} and d_{clent} , respectively.

In order to make use of the ‘neutral membrane’ principle, we have to define this ‘central surface’ at height

$$z_{cent}(r_x) = z_{cp}(r_x) + q(z_{ca}(r_x) - z_{cp}(r_x)), \quad 0 \leq q \leq 1, \quad (2.4)$$

where q defines the relative position of this neutral membrane inside the cornea. $q = 0$ corresponds to the posterior cornea and $q = 1$ to the anterior cornea. The value of q depends on material properties like density and the structural composition of the corneal tissue. Since the area of this central surface will be conserved

Table 1: List of parameters considered in our model.

Symbol	Master value	Description
r_{ca}	7.81 mm	Curvature radius of the anterior cornea
r_{cp}	6.83 mm	Curvature radius of the posterior cornea
k_{cp}	9.19 1/m	‘Optical distance’ between the anterior and posterior cornea, see Eq. (3.1)
d_{cc}	0.543 mm	Central thickness of the cornea at vertex
n_c	1.3765	Refractive index of corneal tissue
$r_{x,limb}$	6.50 mm	Half limbus diameter, radial distance of limbus to vertex
r_{cap}	7.54 mm	Curvature radius of the cap/upper cut
k_{cap}	2.29 1/m	‘Optical distance’ between the anterior cornea and the cap/upper cut, see Eq. (3.1)
R_{cap}	4.2 mm	Half diameter of the cap/upper cut, radial distance to the vertex
TZ	3.7 mm	Half diameter of the transition zone, intersect of lenticule boundary/lower cut and cap/upper cut
d_{ccap}	0.135 mm	Central thickness of the cap/flap at vertex
D_{plan}	−5 dpt	Aimed refractive power change
r_{PI}	20 mm	Curvature radius of the patient interface (PI)
q	0.60	Relative thickness (from posterior cornea)
θ	90°	Incision angle between tangent on the anterior cornea and tangent of the incision

¹ Note, that for an astigmatic cornea two 2D slices can be plotted. One of each at minimal and maximal curvature radius.

under deformations, we use it as reference points to describe the rest of the profiles inside the cornea. Therefore, a local reference frame on the central surface is defined as $(\vec{x}_{T,r_x}, \vec{x}_{T,\phi}, \vec{x}_N)$

$$\vec{x}_{T,r_x} = \frac{\partial_{r_x} \vec{x}_{\text{cent}}}{\left\| \partial_{r_x} \vec{x}_{\text{cent}} \right\|} = \frac{1}{\sqrt{1+z_{\text{cent}}'^2}} \begin{pmatrix} \cos(\phi) \\ \sin(\phi) \\ z_{\text{cent}}' \end{pmatrix},$$

$$\vec{x}_{T,\phi} = \frac{\partial_{\phi} \vec{x}_{\text{cent}}}{\left\| \partial_{\phi} \vec{x}_{\text{cent}} \right\|} = \begin{pmatrix} -\sin(\phi) \\ \cos(\phi) \\ 0 \end{pmatrix}, \quad (2.5)$$

$$\vec{x}_N = \frac{\partial_{r_x} \vec{x}_{\text{cent}} \times \partial_{\phi} \vec{x}_{\text{cent}}}{\left\| \partial_{r_x} \vec{x}_{\text{cent}} \times \partial_{\phi} \vec{x}_{\text{cent}} \right\|}$$

$$= \frac{1}{\sqrt{1+z_{\text{cent}}'^2}} \begin{pmatrix} -z_{\text{cent}}' \cos(\phi) \\ -z_{\text{cent}}' \sin(\phi) \\ 1 \end{pmatrix}, \quad (2.6)$$

where \vec{x}_{T,r_x} and $\vec{x}_{T,\phi}$ denote unit tangent vectors in r_x - and ϕ -direction and \vec{x}_N the normal vector on the central surface. Using 3D coordinates, a profile p can be parametrized by

$$\vec{x}_p(r_x) = \vec{x}_{\text{cent}}(r_x) - d_p(r_x) \vec{e}_z,$$

$$d_p(r_x) = z_{\text{cent}}(r_x) - z_p(r_x), \quad (2.7)$$

and in the local reference frame by

$$\vec{x}_p(r_x) = \vec{x}_{\text{cent}}(r_x) - \frac{d_p(r_x)}{\sqrt{1+z_{\text{cent}}'^2}} \left[z_{\text{cent}}' \vec{x}_{T,r_x} + \vec{x}_N \right]. \quad (2.8)$$

Here we constructed a profile p starting from the neutral membrane and adding a distance $d_p(r_x)$ in z -direction. A basic property of our model, cf. Figure 6, is that the local components $(\vec{x}_{T,r_x} \cdot \vec{e}_z, \vec{x}_{T,\phi} \cdot \vec{e}_z, \vec{x}_N \cdot \vec{e}_z)$ are conserved under deformations. This can be interpreted as follows. The interior of the cornea is transformed with respect to its location in relation to the central surface, based on the initial position for a non-deformed/natural cornea. If we now define the deformed state of the cornea, based on a change from $z_{\text{cent,pre}}$ to $z_{\text{cent,post}}$, we arrive at the following expression

$$\vec{x}_{p,\text{post}}(r_{x,\text{post}}) = \vec{x}_{\text{cent,post}}(r_{x,\text{post}}) - \frac{d_p(r_{x,\text{pre}})}{\sqrt{1+z_{\text{cent,pre}}'^2}}$$

$$\left[z_{\text{cent,pre}}' \vec{x}_{T,r_x,\text{post}} + \vec{x}_{N,\text{post}} \right]. \quad (2.9)$$

The parameters $r_{x,\text{pre}}$ and $r_{x,\text{post}}$ define the r_x values of parametrized points on the central surface before and after the transformation. In addition to this equation, based on

the definition of the local reference frame of the central surface, we can now add the restriction of the conserved area of the neutral membrane. Formally, it is the following integral equation²

$$A_{\text{pre}} = 2\pi \int_0^{r_{x,\text{pre}}} \rho \sqrt{1+z_{\text{cent,post}}'(\rho)^2} d\rho$$

$$= 2\pi \int_0^{r_{x,\text{post}}} \rho \sqrt{1+z_{\text{cent,post}}'(\rho)^2} d\rho = A_{\text{post}}. \quad (2.10)$$

Next, we implement our ansatzes of parabolic profiles. The advantage compared to spherical profiles is that sums of polynomials are again polynomials. Therefore, we can also assume

$$z_{\text{cent,pre/post}}(r_x) = z_{0,\text{cent,pre/post}} - \frac{r_x^2}{2r_{\text{cent,pre/post}}}. \quad (2.11)$$

with this definition, the area restriction Eq. (2.10) and the two component equations of Eq. (2.9) can be simplified to

$$A_{\text{pre/post}}(r_{x,\text{pre/post}}) = \frac{2\pi}{3} r_{\text{cent,pre/post}}^2$$

$$\left(\left(1 + \frac{r_{x,\text{pre/post}}^2}{r_{\text{cent,pre/post}}^2} \right)^{\frac{3}{2}} - 1 \right), \quad (2.12)$$

$$\Rightarrow r_{x,\text{post}}(r_{x,\text{pre}}) = r_{\text{cent,post}}$$

$$\sqrt{\left(1 + \frac{r_{\text{cent,pre}}^2}{r_{\text{cent,post}}^2} \left(\left(1 + \frac{r_{x,\text{pre}}^2}{r_{\text{cent,pre}}^2} \right)^{\frac{3}{2}} - 1 \right) \right)^{\frac{2}{3}} - 1}, \quad (2.13)$$

$$r_{x,p,\text{post}}(r_{x,\text{post}}) = r_{x,\text{post}} + \frac{d_p(r_{x,\text{pre}})}{\sqrt{r_{\text{cent,pre}}^2 + r_{x,\text{pre}}^2} \sqrt{r_{\text{cent,post}}^2 + r_{x,\text{post}}^2}}$$

$$\left[r_{x,\text{pre}} r_{\text{cent,post}} - r_{x,\text{post}} r_{\text{cent,pre}} \right], \quad (2.14)$$

$$z_{p,\text{post}}(r_{x,p,\text{post}}) = z_{\text{cent,post}}(r_{x,\text{post}})$$

$$- \frac{d_p(r_{x,\text{pre}})}{\sqrt{r_{\text{cent,pre}}^2 + r_{x,\text{pre}}^2} \sqrt{r_{\text{cent,post}}^2 + r_{x,\text{post}}^2}}$$

$$\left[r_{x,\text{pre}} r_{x,\text{post}} + r_{\text{cent,pre}} r_{\text{cent,post}} \right]. \quad (2.15)$$

with Eqs. (2.14) and (2.15) we can set up an implicit equation for $z_{\text{cent,post}}$ that can be solved numerically. We simply identify the profile of the anterior cornea with the one of the PI

² The factor of 2π arises from the integral over ϕ . For astigmatic corneas, the integrand has to be extended to derivatives with respect to ϕ .

$$z_{ca, post}(r_{x, ca, post}) = z_{PI}(r_{x, ca, post}), \quad (2.16)$$

and solve for $r_{cent, post}$. This describes the eye in the state docked to the PI. The curvature radius of the central surface before the deformation can be obtained by

$$\begin{aligned} z_{cent, pre}(r_x) &= z_{0, cent, pre} - \frac{r_x^2}{2r_{cent, pre}} \\ &= (q-1)d_{cc} - \frac{r_x^2}{2} \left(\frac{q}{r_{ca}} + \frac{1-q}{r_{cp}} \right) \Rightarrow \frac{1}{r_{cent, pre}} \\ &= \left(\frac{q}{r_{ca}} + \frac{1-q}{r_{cp}} \right). \end{aligned} \quad (2.17)$$

In Figure 1, both states of the free and docked cornea are presented for a certain choice of parameter values. We use Python as our coding and graphics environment.

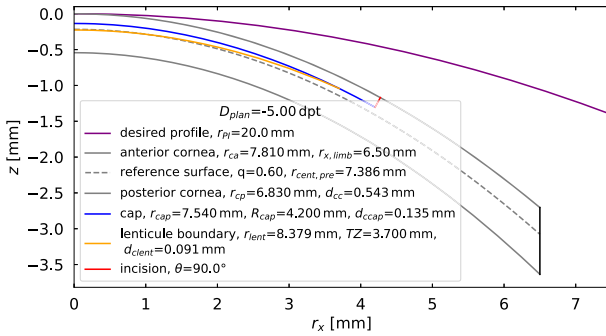
By design, the endpoints of the cornea can move freely while obeying Eq. (2.9) from Figure 1A to B. This is valid for a free corneal tissue that is adapting to a desired profile, the PI. In contrast, in reality, the cornea of an eye that is docked to the PI is not exhibiting free endpoints. Therefore,

our model also consists of the following consequent transformation.

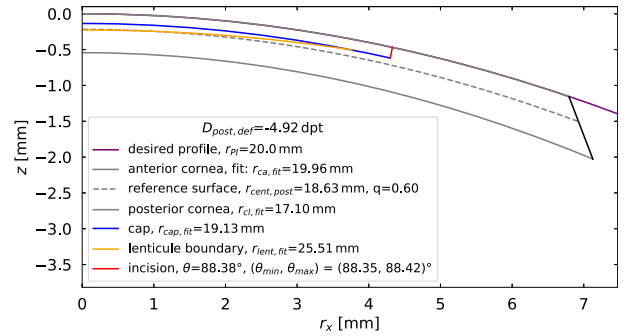
Since at some radial distance the cornea is fixed in position, we introduce a rescaling that brings the endpoints of the deformed free cornea back to their initial position. We suggest this to happen at the limbus at about $r_{x, limb} = 6.5$ mm. Since we still focus on a 2D transformation, i.e., the transformation of the neutral membrane, also the rescaling, is based on areas. For the profiles of the anterior/posterior cornea and the central surface, we fit second order polynomials. The ratio of the area before and after the rescaling defines the scaling factor κ . For simplicity, we assume the curvature radii to be conserved during rescaling. For

$$\begin{aligned} z_{fit}(r_x, r_{fit}) &= z_{0, fit} - \frac{r_x^2}{2r_{fit}}, A(r_x, r_{fit}) \\ &= \frac{2\pi}{3} r_{fit}^2 \left(\left(1 + \frac{r_x^2}{r_{fit}^2} \right)^{\frac{3}{2}} - 1 \right), \end{aligned} \quad (2.18)$$

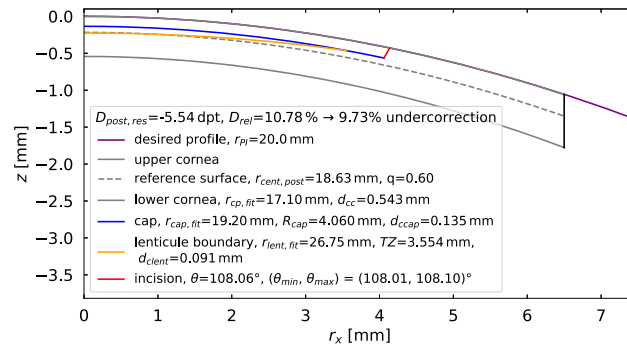
we can define



(A) pre 2D deformation



(B) post 2D deformation free end



(C) post 2D deformation fixed end

Figure 1: In (A) the cornea is shown in its normal state, whereas in (B) the cornea is docked to the PI with free ends and in (C) with fixed ends at constant r_x .

$$\kappa = \frac{A(r_{x,\text{end}}, r_{\text{fit}})}{A(r_{x,\text{limb}}, r_{\text{fit}})} = \frac{A(r_{x,\text{pre, res}}, r_{\text{fit}})}{A(r_{x,\text{post, res}}, r_{\text{fit}})}, \quad (2.19)$$

$$r_{x,\text{post, res}} = r_{\text{fit}} \sqrt[3]{\left(1 + \frac{1}{\kappa} \left(\left(1 + \frac{r_{x,\text{pre, res}}^2}{r_{\text{fit}}^2}\right)^{\frac{3}{2}} - 1 \right) \right)^{\frac{2}{3}}} - 1, \quad (2.20)$$

for each of the three profiles. For other profiles like the cap, lenticule boundary and the incision, we define their position with respect to their relative location within the cornea before the deformation

$$r_{x,p,\text{post, res}} = r_{x,\text{cp, post, res}} + \frac{z_p(r_{x,\text{pre}}) - z_{\text{cp}}(r_{x,\text{pre}})}{z_{\text{ca}}(r_{x,\text{pre}}) - z_{\text{cp}}(r_{x,\text{pre}})} (r_{x,\text{ca, post, res}} - r_{x,\text{cp, post, res}}), \quad (2.21)$$

$$z_{p,\text{post, res}} = z_{\text{cp, post, res}} + \frac{z_p(r_{x,\text{pre}}) - z_{\text{cp}}(r_{x,\text{pre}})}{z_{\text{ca}}(r_{x,\text{pre}}) - z_{\text{cp}}(r_{x,\text{pre}})} (z_{\text{ca, post, res}} - z_{\text{cp, post, res}}). \quad (2.22)$$

As a result of all these transformations, we obtain Figure 1C, displaying the transformation of the cornea with fixed endpoints at $r_{x,\text{limb}}$. The diopters planned for a free cornea before docking to the PI are given in Figure 1A as an initial parameter denoted by D_{plan} . Afterwards, the change in refractive power is computed by

$$D = (n_c - 1) \left(-\frac{1}{r_{\text{cap}}} + \frac{1}{r_{\text{lent}}} \right). \quad (2.23)$$

D_{rel} of Figure 1C is defined as $D_{\text{rel}} = \frac{D_{\text{post, res}}}{D_{\text{plan}}} - 1$, where $n_c = 1.3765$ is the refractive index of the cornea. In Figure 1C, we realize that for this parameter choice we would expect an undercorrection of about 9.73% if 100% are planned for a cornea docked to the PI. This is already a hint in the direction towards 9–16% undercorrection described in [6, 10–12].

Another improvement of the estimation of corneal deformation in our model is the description of the closing

of the lenticule by the same mathematics as explained above. The anterior cornea is still the upper profile of the moving tissue, whereas the lower profile is now the cap/upper cut itself.

In Figure 2, the closing of the lenticule is presented. Here, the change in refractive power is computed from the change in curvature of the anterior cornea

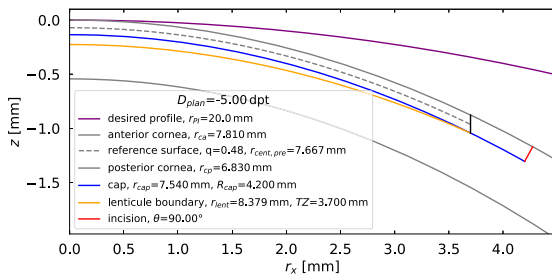
$$D = (n_c - 1) \left(\frac{1}{r_{\text{ca, post}}} - \frac{1}{r_{\text{ca, pre}}} \right). \quad (2.24)$$

From this part of our model, we expect 3.44% undercorrection compared to the planned refractive power change for a free cornea. In total, starting from 100% planned for a docked cornea, we arrive at an undercorrection of 12.82% after the closing of the lenticule. In Appendix B, residuals of the fits of the previously described models are shown. Overall, the deviation is of the order of the spot size of the surgical femtosecond laser.

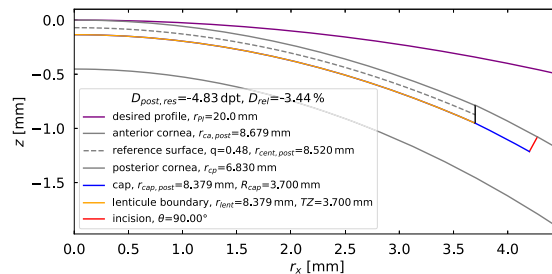
In order to test different possible patient scenarios, a variation of various parameters is performed in Sections 3.1 and 3.2.

Table 2: List of parameter values considered for the model test. Bold numbers represent the ‘master value’ of a parameter.

r_{ca} [mm]	6.86	7.30	7.81	8.61	9.59
k_{cp} [1/m]	-2.67	3.27	9.19	13.62	18.08
$r_{\text{cp}}(k_{\text{cp}}, r_{\text{ca}})$ [mm] (see Eq. (3.1))	6.09	6.44	6.83	7.43	8.15
d_{cc} [mm]	0.400	0.480	0.543	0.600	0.650
$r_{x,\text{limb}}$ [mm]	6.00	6.25	6.50	6.75	7.00
k_{cap} [1/m]	-7.52	-3.63	2.29	6.70	11.17
$r_{\text{cap}}(k_{\text{cap}}, r_{\text{ca}})$ [mm] (see Eq. (3.1))	6.65	7.07	7.54	8.28	8.85
R_{cap} [mm]	3.7	4.0	4.2	4.5	4.9
TZ [mm]	3.0	3.3	3.7	3.9	4.2
d_{ccap} [mm]	0.100	0.120	0.135	0.150	0.160
D_{plan} [dpt]	-1	-3	-5	-7	-9
r_{PI} [mm]	10	15	20	30	999
q	0.15	0.30	0.45	0.60	0.80
θ [°]	45	68	90	112	135



(A) pre 2D closing lenticule



(B) post 2D closing lenticule

Figure 2: From (A) to (B) the lenticule is closed by the same mathematical formalism as used before in Figure 1.

3 Results

In the previous section, the mathematical description of the docking to the PI and closing of the lenticule is defined. In the following, an analysis by a variation of multiple parameters is performed.

3.1 Model application– docking to PI

In this section, we partially evaluate the parameter space of the deformation model described in Section 2. It turned out to be practical to introduce alternative variables for the curvature radii of the cap and posterior

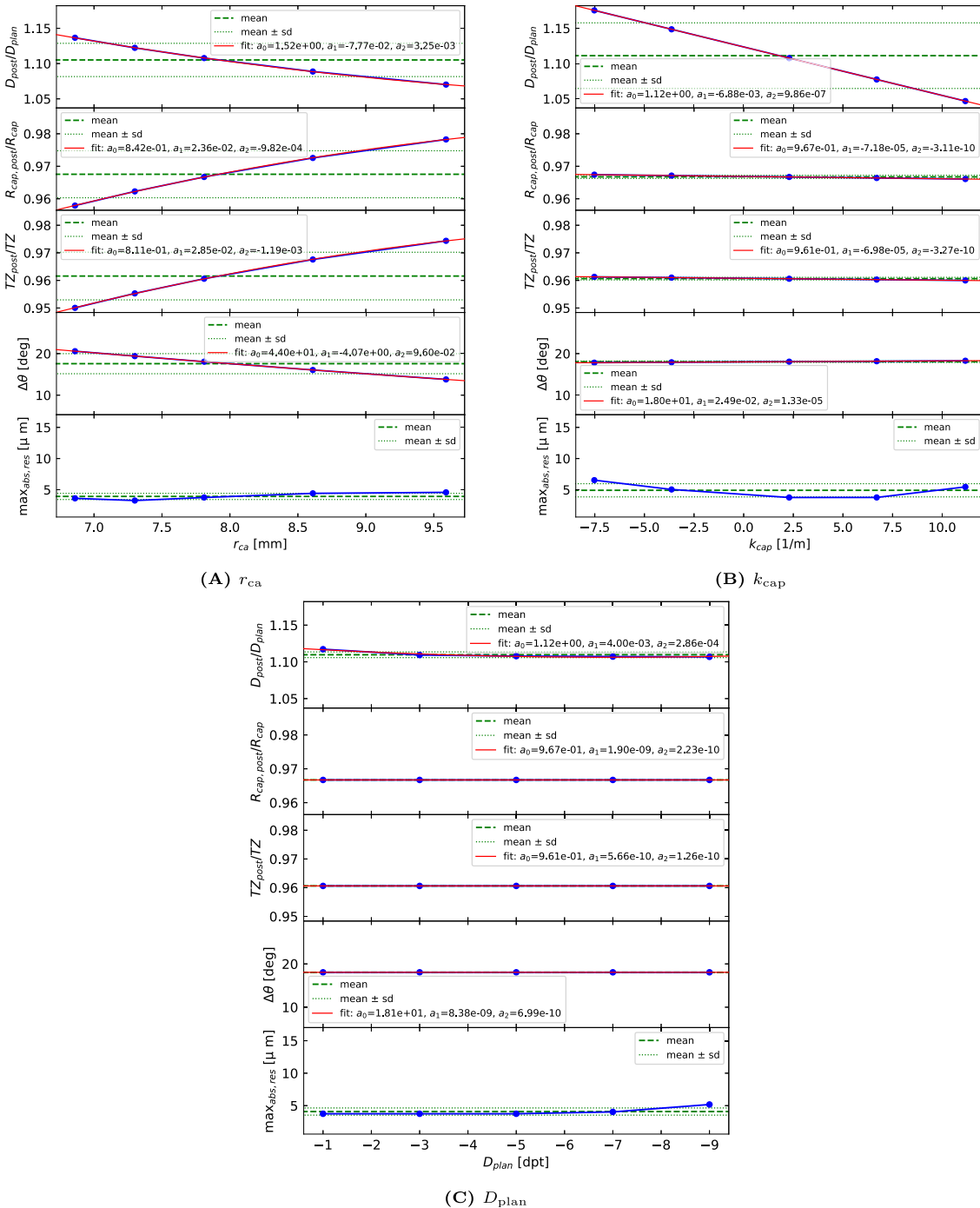


Figure 3: Docking to PI, Section 3.1. Various parameter variations for the ratio of D_{post}/D_{plan} , $R_{cap,post}/R_{cap}$ and TZ_{post}/TZ , the deviation in incision angle $\Delta\theta$ and maximal absolute fit residue $\max_{abs,res}$. In order to model the ratios and the deviation in incision angle, second order polynomials $y_a(x) = a_0 + a_1x + a_2x^2$ are fitted to the five scenarios.

cornea. Their ‘optical distances’ to the anterior cornea are defined as

$$k_{\text{cap/cp}} = \frac{1}{2} \left(\frac{1}{r_{\text{cap/cp}}} - \frac{1}{r_{\text{ca}}} \right). \quad (3.1)$$

The choice of parameter values is presented in Table 2.

As defined in Eq. (2.4), $q = 0$ represents the posterior cornea and $q = 1$ the anterior cornea. For each parameter, we define a so-called ‘master value’ and four additional values. These values should be related to standard eyes that are found in society [23–29]. To keep computation time low, we only varied one parameter at a time while keeping the others fixed at their master value. A selection of variations is given in Figure 3, whereas the rest is listed in Appendix C.

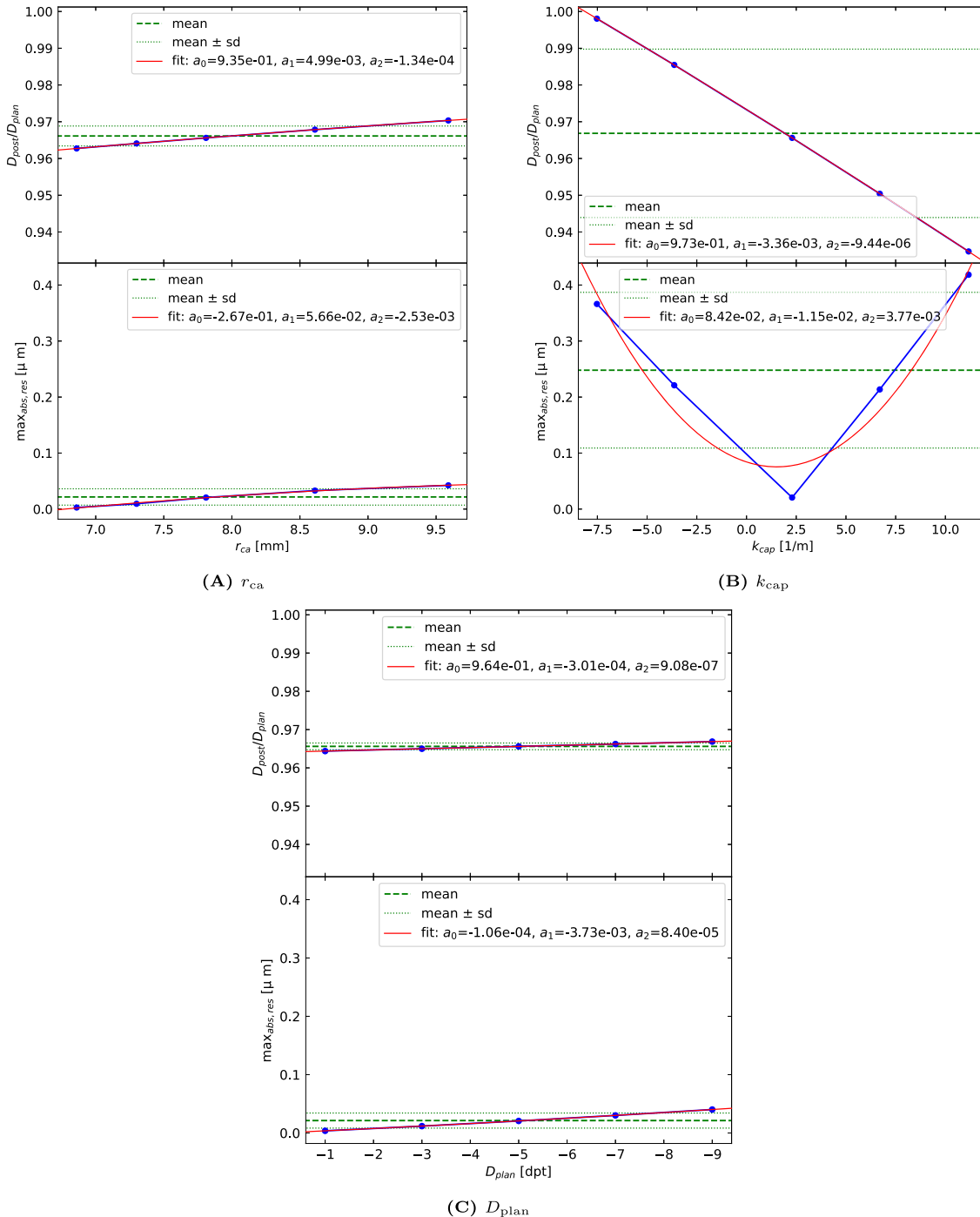


Figure 4: Closing lenticule, Section 3.2. Various parameter variations for the ratio of $D_{\text{post}}/D_{\text{plan}}$ and maximal absolute fit residue $\max_{\text{abs,res}}$. In order to model the ratio, second order polynomials $y_a(x) = a_0 + a_1x + a_2x^2$ are fitted to the five scenarios.

3.2 Model application – closing lenticule

Similar to Section 3.1, an analysis of various parameter value choices is performed for the model describing the closing of the lenticule. The choices of parameter values for r_{ca} , k_{cap} , TZ , d_{ccap} and D_{plan} are identical to the ones defined in Table 2. Only for q we chose a different set, $q \in \{0.36, 0.44, 0.48, 0.52, 0.60\}$, since the cap consists of a different composition of layers than the full cornea, where $q = 0$ represents the cap and $q = 1$ the anterior cornea. Therefore, since, e.g., the density distribution is different to Section 3.1, also the neutral membrane of the corneal cap is located at a different relative thickness with respect to the cut.

Like before in Section 3.1, we only vary one parameter at a time while keeping the others fixed at their master value. A selection of variations is given in Figure 4, whereas the rest is listed in Appendix C.

4 Discussion

We modeled the ratio D_{post}/D_{plan} for both the docking and the closing of the lenticule. Combining both steps, we obtain the chains of D values below. The predictions of the model provide the following exemplary estimate:

	closed lenticule	\rightarrow	free cornea	\rightarrow	docked to PI
model:	-4.83 dpt		-5.00 dpt		-5.54 dpt
rel. D (rel. deviation):	87.18 % (-12.82%)	\leftarrow	90.25 % (-9.75%)	\leftarrow	100 %

Reading this chain from right to left, one can interpret the undercorrection emerging from the nominal value, which is defined under docking (100%), to the output value that is achieved after the lenticule has closed (87.18%). In contrast, reading this chain from left to right, one can interpret the compensation based on the nominal value which is aimed after the lenticule has closed, finally reaching the output value that is the value used under docking. This corresponds to the general interpretation as described in [10].

Since we did no comparison to patient data on an individual basis yet, we do not know the numerical applicability of our model to reality. This is one of the near future steps we will investigate. Nevertheless, the corridor of 9–16% undercorrection [6, 10–12] is achieved.

It is important to understand how the established corneal deformation model can be used in the prediction of the refractive effect in the postoperative cornea. The first thing one should know is whether the system in use has any corneal deformation model built in. Similarly, one should also know whether the system in use comprises any empirical nomogram whether or not visible to the user, at least for the refractive power of the correction.

Provided this is not the case, i.e., no corneal deformation model or non-visible nomogram is already built in, one can apply the particular model to determine all geometric and refractive deviations. These include the impact of docking on the resulting lenticule shape (both power and diameter); the impact of docking on the resulting cap shape (diameter); the impact of docking on the resulting incision (angulation) as well as the impact of reflecting/repositioning the cap on the anterior corneal shape (refractive power).

However, the overall provided values shall serve, at least, as a ball-park figure to check and refine the planning parameters of the treatment. Important aspects are the impact of docking on the resulting lenticule shape, e.g., an increase of +11% for power (~ 0.5 dpt) and decrease of -3% in diameter (~ 0.2 mm). Moreover, the impact of docking on the resulting cap shape, e.g., a decrease of -4% in diameter (~ 0.3 mm), on the resulting incision (increase angulation by +18°) as well as the impact of reflecting/repositioning

the cap on the anterior corneal shape, e.g., an increase of another +3.5% of the refractive power (~ 0.25 dpt).

As mentioned before in the beginning of Section 2, our model is restricted to rotational symmetric corneas, i.e., non-astigmatic. Even if the local curvature radius of an astigmatic cornea of the form,

$$z_{ast}(r_x, \phi) = \sqrt{r_{sph}^2 - r_x^2} - r_{sph} + \sqrt{r_{cyl}^2 - \sin^2(\phi - \phi_0)r_x^2} - r_{cyl} \approx -\frac{r_x^2}{2} \left(\frac{1}{r_{sph}} + \frac{\sin^2(\phi - \phi_0)}{r_{cyl}} \right), \quad (4.1)$$

is non-trivial, one could simply apply our model to both the cornea with minimum and maximum curvature radius separately. Therefore, as a first step of estimation, one could

combine the model predictions obtained for the two ‘sub scenarios’ to determine the effects of refractive astigmatism or corneal toricity. Moreover, the magnitude of the toricity is in general far below $\pm 10\%$ of the total refractive power of the cornea with about 43 dpt and therefore less influential. We have used a reduced model with rotational symmetry as an initial approach in order to reduce the mathematical complexity of the expressions. This shall serve us to determine the feasibility of the model, which could be then extended to more general corneal geometries and morphologies. The typical corneal toricity (~ 1 dpt) represents merely $\sim 2\%$ of the corneal curvature ~ 43 dpt, so that astigmatic effects are expected to correspond to a second order correction beyond the basic rotational symmetric effect.

A simple approach to deal with astigmatic shapes (whether these are, e.g., corneal toricity, or a spherocylindrical correction) would involve determining the meridional curvatures of the two principal meridians of the cornea, given by, e.g., the keratometry readings of the cornea at two main meridians perpendicular to each other. Moreover, the meridional corrections of the two principal meridians of the treatment are defined by spherical and cylindrical refractive defects which are to be corrected. Our model is then applied twice, once for each pair of values corresponding to the same meridian. One time for the flat meridian (and corresponding meridional correction power) and another time for the steep meridian (and corresponding meridional correction power).

With the obtained model predictions, the overall treatment effect can be composited back to sphero-toric surfaces providing a reasonable estimate.

The model we have up to now, described in this paper, originated from a discrete ‘mesh’ version. The central surface was considered to be sliced in concentric conical ring surfaces (CCRS), whereas each CCRS area was kept constant. The remaining profiles of, e.g., anterior cornea, cap and lenticule boundary are defined via constant ‘distance’ and angle to the central surface, similar to the reference frame in Eqs. (2.5) and (2.6). The fit procedure of aligning the anterior surface of the cornea was based on the set of tilt angles of each CCRS. The computation time for about 20 mesh points is about a factor of 100–1000 longer than the one for the continuous model. The fit procedure of the model described in this paper is basically limited to the determination of the curvature radius of the central surface.

Nevertheless, the fit of parabolic surfaces to profiles like the cap and lenticule boundary seems to be acceptable by considering the residuals for Figures 1B, C and 2B presented in Figure 7. For the graphics Figure 1B and C, the residuals Figure 7A and B are below $\pm 4 \mu\text{m}$ which is of the order of the spot size of a surgical femtosecond laser. For Figure 2B, the residuals Figure 7C are even one order of magnitude smaller.

Therefore, we can consider the profiles to be described by parabolas even after deformation and rescaling. One could speculate that the shape of the residuals hints spherical aberration errors.

Comparing Figure 1B with Figure 1C, the main influence on the ratio $D_{\text{post}}/D_{\text{plan}}$ seems to originate from the rescaling and not the deformation of the free corneal tissue. We assumed the cornea to be fixed at limbus. In reality, the sclera is not rigid, and its stiffness is not modeled in this paper. The rescaling along the same ‘macroscopic’ radius of curvature together with the conservation of the area, ‘microscopically’ results in folds in the corneal tissue. Furthermore, we chose a vertical line for the intersection between the cornea and the sclera in our simple model. In the future, more physiological shapes of this intersection could be evaluated. Nevertheless, the influence is expected to be low, since because the thickness of the cornea is small compared to $r_{x,\text{limb}}$, the center of the intersection is more important than the actual shape around this center. By comparing Figure 1 with Figure 2, the contribution of the closing of the lenticule is smaller than the actual deformation due to the docking to the PI.

The cap collapses onto the stromal bed, after the lenticule has been removed. This does create the refractive change. The anterior cornea (the cap between the anterior cut and the anterior cornea) is the moving tissue, and the posterior cornea (the residual stroma below the posterior cut) is the ‘fixed’ tissue. In reality, though, both will likely move (although the anterior shall move relatively much more down, compared to what the posterior moves up). The relative contribution of the cap moving down and the residual stroma moving up can be estimated from the ratio of the following products. The first product is the amount of tissue in the cap (defined by, e.g., thickness or volume) times some sort of biomechanical resistance (this can be, e.g., Young modulus or tensile strength). The second product consists of the amount of tissue in the residual stroma times its biomechanical parameter.

In Table 3 we present qualitative results of our model, based on Figures 3 and 4, and compare them with results in [11]. In [11], lenticule extraction treatments of 2564 eyes from three different countries were analyzed. For r_{ca} , TZ and d_{ccap} , the qualitative result of [11] and our model coincide. For d_{cc} , R_{cap} and D_{plan} (marked with *), no significant discrepancy can be found.³ For the parameters

³ Official diopter measurements are performed with a step size of 0.25 dpt, which corresponds to about $\pm 5\%$ uncertainty for 5 dpt planned refractive power change and about $\pm 2\%$ uncertainty for 12 dpt. Therefore, it is acceptable to say that a contribution to the ratio of $D_{\text{post}}/D_{\text{plan}}$ below about $\pm 2\%$ can be classified as not significant. Even for large cohorts like in [11], it is hard to reach significance.

Table 3: Qualitative results of our model Figures 3 and 4 compared to [11]. *For d_{cc} , R_{cap} and D_{plan} , no significant discrepancy can be found.

Input	D_{post}/D_{plan}	$R_{cap,post}/R_{cap}$	TZ_{post}/TZ	$\Delta\theta$
r_{ca}	Steeper cornea = higher under-correction (uc.)	Steeper cornea = larger cap	Steeper cornea = larger TZ	Steeper cornea = larger angle deviation (dev.)
d_{cc}^*	Thinner cornea = higher uc.	–	–	Thinner cornea = larger angle dev.
R_{cap}^*	Larger cap = higher uc.	Larger cap = smaller cap	–	Larger cap = larger angle dev.
TZ	Larger lenticule = less uc.	–	Larger lenticule = smaller lenticule	–
d_{ccap}	Thicker cap = higher uc.	–	–	–
D_{plan}^*	Higher correction = less uc.	–	–	–

anterior curvature radius r_{ca} , radius of the lenticule TZ and the central thickness of the cap d_{ccap} , our observations coincide with observations in [11]. For d_{cc} Figure 9A, we have to note that a trend in undercorrection is significant but rather small. Moreover, in [11], where no significant trend has been found, the pachymetry lies between 482 and 663 μm which is a narrower range than we analyzed. For the cap radius R_{cap} , we have to mention that in our model R_{cap} and TZ were varied independently, whereas in reality, i.e., [11], both parameters are rather collinear. This could result in the fact that R_{cap} shows low significance also in reality. For the parameter D_{plan} , we analyzed its relative change. But if we consider the absolute change in diopters, we would conclude to the same result as in [11], where both relative and absolute diopter changes are referred to. Overall, our model seems to fit quite well to the qualitative description of real treatments presented in [11].

During the model building phase, we were also considering spherical caps as mathematical descriptions for profiles like anterior/posterior cornea, cap and lenticule boundary. As described in Eq. (2.3), both mathematical descriptions can be referred to each other via the curvature radius of the profile. The consideration of spherical cap profiles lead to the same qualitative results while increasing the mathematical complexity.⁴ Another modification we tested is to not consider area conservation of the central surface as motivated by the idea of the neutral membrane but following the length conservation as in the 1D neutral axis model. This idea was motivated by the fiber structure of the corneal tissue that is influencing the deformation. Nevertheless, we decided for the model inspired by the neutral membrane, since even if the cornea is constructed by

fibers, these fibers are forming a 2D grid of tissue. This tissue is then assumed to rather behave as an anisotropic material under 2D deformations than a 1D material. Since our goal was to set up a mathematically simpler model than, e.g., FEM simulations, that can respect anisotropy, we did not implement any anisotropic behavior in our model. Even though, it shows the potential of partially compensating the observed undercorrection of [6, 10–12]. As mentioned before, this has to be numerically validated by a comparison to patient data.

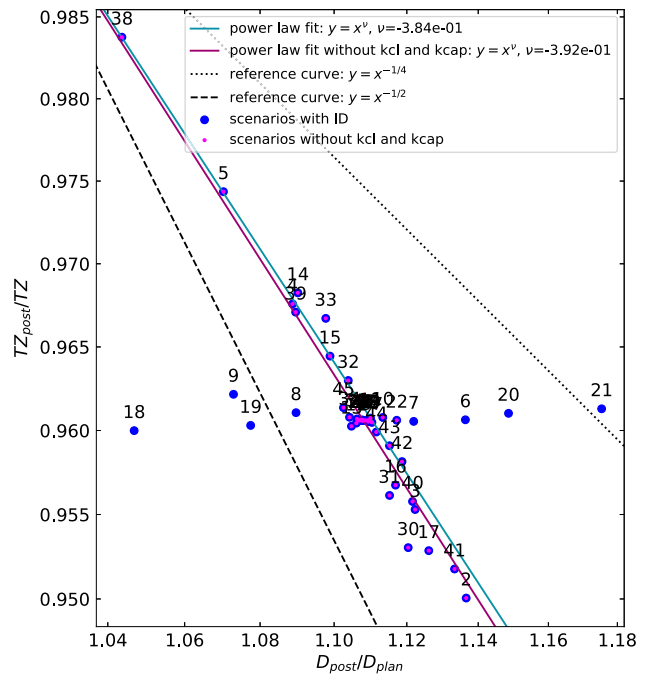


Figure 5: Log-log plot of the relation between the ratio of radial distance of the lenticule TZ_{post}/TZ and the ratio in refractive power change D_{post}/D_{plan} . The dotted curve corresponds to the model of conserved volume, i.e., $s_{x/y} = s_D^{1/4}$, whereas the dashed curve denotes conserved thickness, i.e., $s_{x/y} = s_D^{1/2}$. Our new model described in this paper is exhibiting an exponent of $-\frac{1}{2} < \nu \approx -(0.384 - 0.392) < -\frac{1}{4}$.

⁴ One example of complexity increase is the following. A sum of two polynomials is again a polynomial, whereas the sum of two spherical caps is in general not a spherical cap. Although, in the latter case, one has the possibility to define a local curvature radius of an effective local spherical cap profile.

In addition, a numerical simulation by FEM based on available models [13] had already been performed (unpublished data) providing qualitatively comparable findings: the refractive power of the lenticules was reduced upon releasing applanation (reduced more for flatter applanations); whereas the size (diameter) of the lenticules increased upon releasing applanation (increased more for flatter applanations). The FEM model, unlike the presented model, further predicted a thinning of the lenticules upon releasing applanation (thinner lenticules after releasing flatter applanations). But the magnitude of the effect predicted by the FEM model was larger than that predicted by the present simplified model.

Corneal biomechanics, including its anisotropic, nonlinear elastic properties and viscoelastic properties, plays an important role in the corneal morphology after operation, in which the cornea experiences a dynamical process, and then affects the refractive effect. From a mechanical point of view, an appropriate corneal mechanical property is needed to provide a detailed modeling level. Our approach was less ambitious and aimed only to provide a simple macroscopic model which may support a basic understanding of the geometric and refractive implications of deforming the cornea under a rigid laser patient interface. A model that is already in use is based on the idea of volume conservation of the corneal

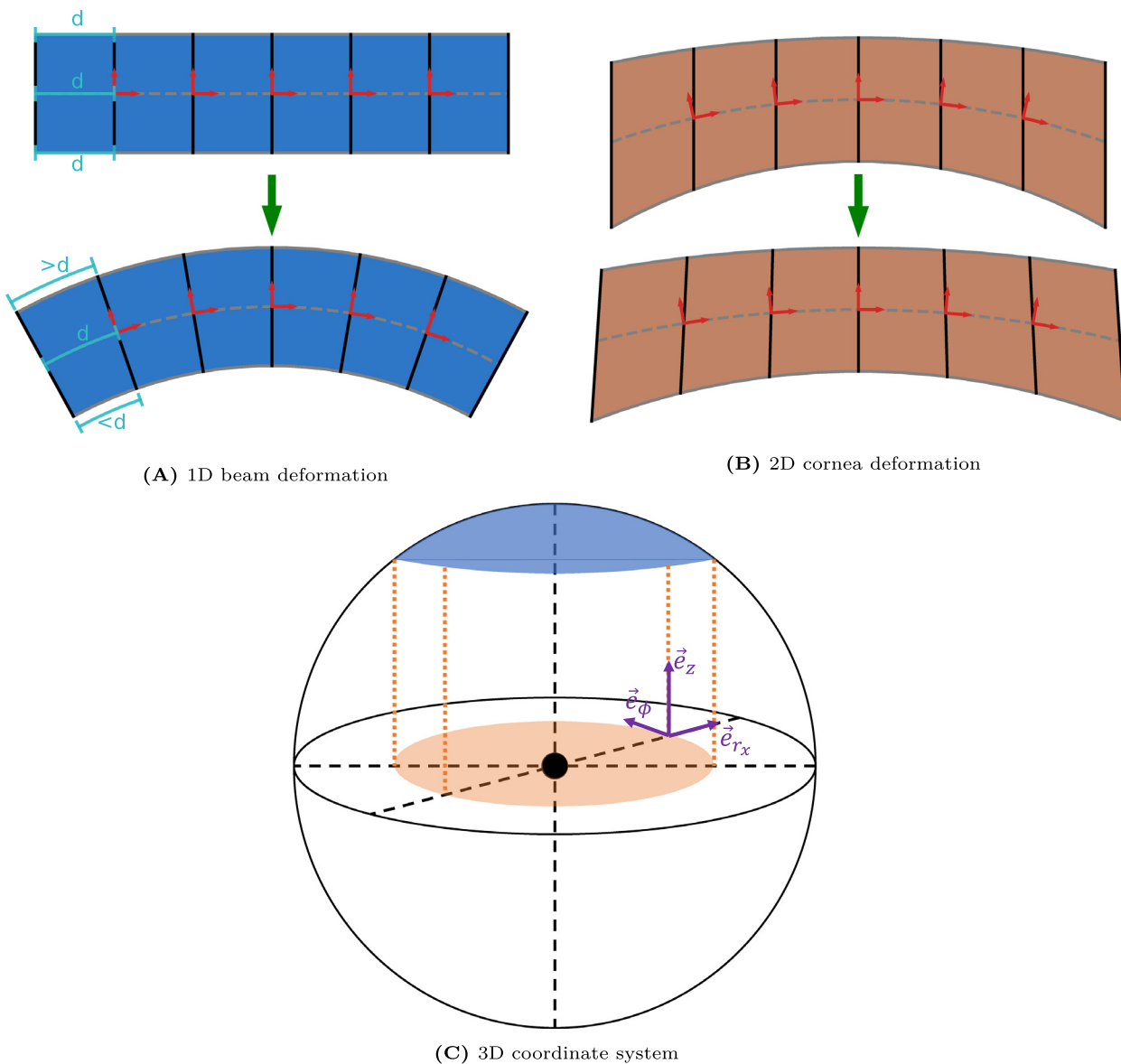


Figure 6: Scheme of different-dimensional deformations of (A) a free beam and (B) a free corneal tissue. (C) Schematically shows the eye visualized as a sphere and the cornea highlighted as a blue cap in 3D.

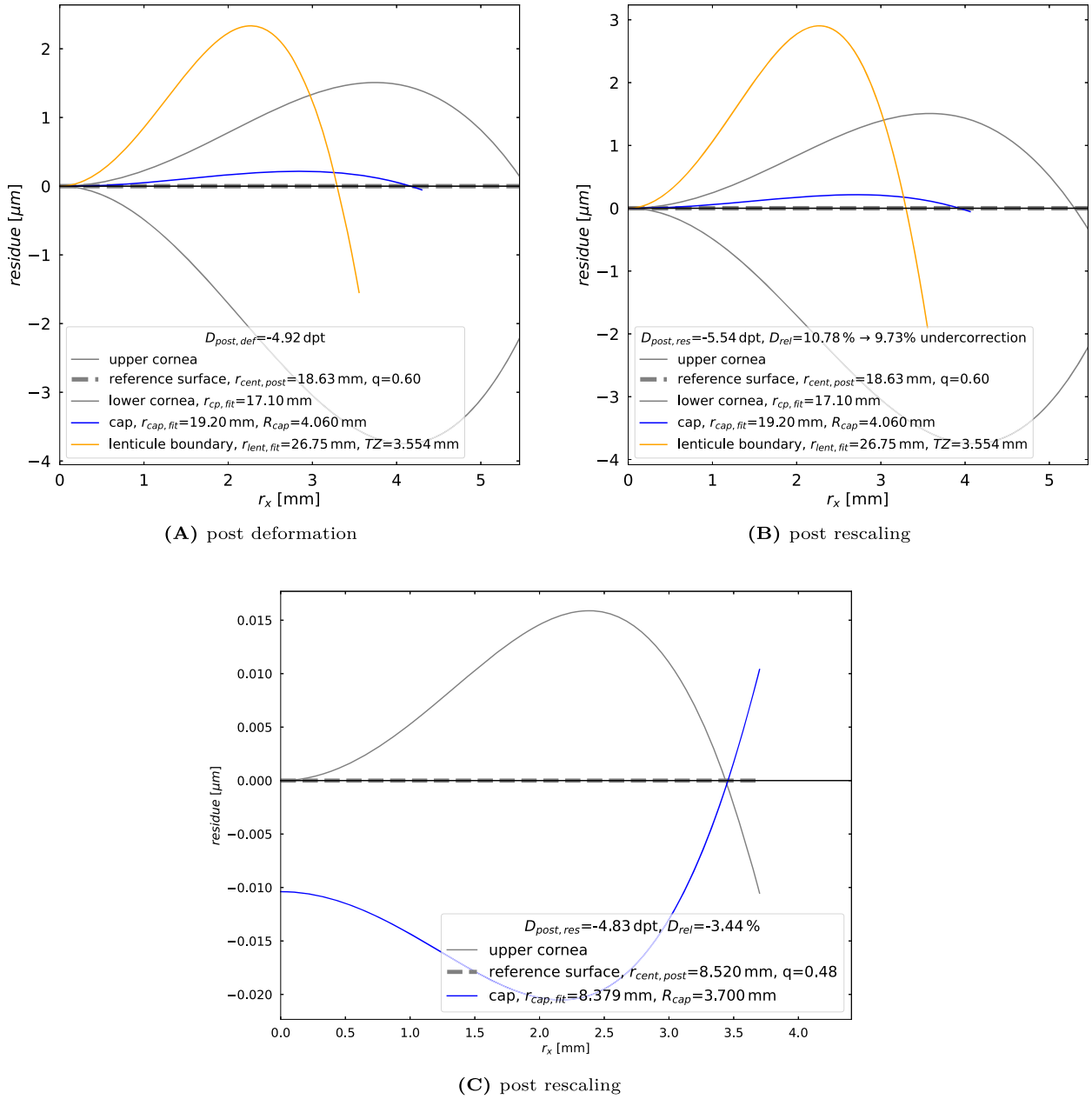


Figure 7: Residuals of various fitted profiles, e.g., cap or lenticule boundary, of Figures 1B, C and 2B.

tissue during deformation, since it is assumed to be incompressible. A sphere is characterized by its curvature radius r . Imagine the vertex of a sphere located at the origin of a coordinate system. In a 2D slice, imagine the right triangle defined by the points $(0, -d)$, $(a, -d)$ and $(0, -r)$. From $(r-d)^2 + a^2 = r^2$, we can obtain the curvature radius to $r = \frac{d^2 + a^2}{2d}$. The refractive power is defined as

$$D = \frac{n-1}{r} = \frac{(n-1)2d}{d^2 + a^2} = \frac{(n-1)2d}{a^2} + \mathcal{O}\left(\left(\frac{d}{a}\right)^3\right), \quad (4.2)$$

which we can approximate by neglecting third order in $\frac{d}{a}$. If we want to achieve a relative refractive power change of $s_D = D_{\text{final}}/D_{\text{initial}} = \frac{s_z}{s_x s_y}$, we could scale the depth of the lenticule by s_z (along z -axis) and the radial distance of the lenticule by $s_{x/y}$ (along x - y -plane). In order to keep the volume constant $1 = s_{\text{vol}} = s_x s_y s_z$, we have to define the scaling factors as $s_z = \frac{1}{s_x s_y}$. For a rotational symmetric scaling $s_x = s_y$ holds. Therefore, the scaling of the refractive power change $s_D = s_z^2 = (s_{x/y})^{-4}$ is equal to the inverse of the one-dimensional scaling factor $s_{x/y}$ to the power of four along

the x - y -plane. Another approach is to define the thickness to be conserved, which leads in this simple approximation to the relation $s_D = (s_{x/y})^{-2}$. Both different functional dependencies of the ratio of the radial distance scaling in the x - y -plane on the ratio of change in refractive power can be compared to the ratio of TZ_{post}/TZ versus the ratio of $D_{\text{post}}/D_{\text{plan}}$. In the log-log plot Figure 5, blue points represent the previously mentioned ratios for several scenarios defined by Table 2. Fitted exponent, $\nu \approx -0.384$, lies between the ones of the other two approaches of keeping volume constant $\nu = -\frac{1}{4}$ and keeping thickness constant ($s_z = 1$) $\nu = -\frac{1}{2}$. A better fit is obtained by discarding the scenarios corresponding to k_{cp} (6–9) and k_{cap} (18–21) from this analysis, i.e., magenta points, since these parameters change the refractive power by almost not influencing the scaling of the lenticule in the x - y -plane.

In Figure 11, the comparison between the initial values of k_{cp} and k_{cap} is compared with their pendant after rescaling. It should give an impression on how different ‘optical distances’/refractive powers in the cornea change due to the docking procedure.

In our model, we assumed a conservation of the area of the neutral membrane. By additionally keeping the thickness constant, we provided also a form of volume conservation which is related to incompressibility, at least around the neutral membrane. In total, the effects of thickness increase anterior to the neutral membrane and thickness decrease posterior to the neutral membrane are assumed to cancel out each other, due to deformation with constant area and volume. Only the location q of the neutral membrane is expected to slightly change. The rescaling is defined by scaling the areas of slices stacked along z -direction. Therefore, the overall density is no longer conserved. This is a way of effectively/implicitly modeling observed undulations at the posterior cornea, see e.g. [30] or <https://www.ebc-europe.com/produit/laser-femto-ldv-z8/>, during applanation in our rigid elastic transformation model. An implementation that can respect the just mentioned behaviors is again FEM. As stated before, we explicitly wanted to obtain a mathematical simpler implementation that can provide enough insights by considering rigid elastic deformations of the corneal tissue only.

5 Conclusions

In contrast to microscopic models of the cornea like FEM [13–19], our model of deformation behavior of the cornea is focused on a rather macroscopic description consisting of rigid and elastic transformations. Nevertheless, we were able to find a simpler mathematical model that could describe the

observed undercorrection as discussed in [6, 10–12]. The numerical prediction accuracy of our model to be used as a compensation before the treatment is performed has to be evaluated in future analysis of patient data.

Future extensions of our model should include astigmatic corneas as well as hyperopic lenticules. Hints on how extensions could look like are already given at some points in this paper.

Acknowledgments: We thank our colleague Pascal Naubereit for a discussion about future improvements of our model.

Author contributions: All the authors have accepted responsibility for the entire content of this submitted manuscript and approved submission.

Research funding: None declared.

Conflict of interest statement: The authors declare no conflicts of interest regarding this article. Both authors were employees of SCHWIND eye-tech-solutions (manufacturer of the SCHWIND ATOS femtosecond laser system for refractive surgery) at the time of this work.

Appendix

A Schematics of deformation

As described in Section 1, our model is inspired by the principle of the ‘neutral axis’, cf. [22]. The schematics of a 1D deformation, e.g., 1D bending of a beam, is presented in Figure 6A. The dashed line represents the ‘neutral axis’ whose length is not changed under the deformation. Other axes that are ‘parallel’ to the ‘neutral axis’ are compressed below and stretched above, see Figure 6A. In contrast, a slice through a cornea that experienced a 2D bending is given in Figure 6B. The schematics of our coordinate system is presented in Figure 6C.

B Residuals

In Figure 7 the residuals of various fitted profiles of Figures 1B, C and 2B are presented.

C Rest of model application

In Figure 8, Figure 9 and Figure 10, the remaining parameter variations in addition to Figure 3 are displayed.

Figure 9B shows almost no influence on output parameters which is in accordance with the results of [31].

For the closing of the lenticule, Figure 12 shows further evaluations in addition to Figure 4.

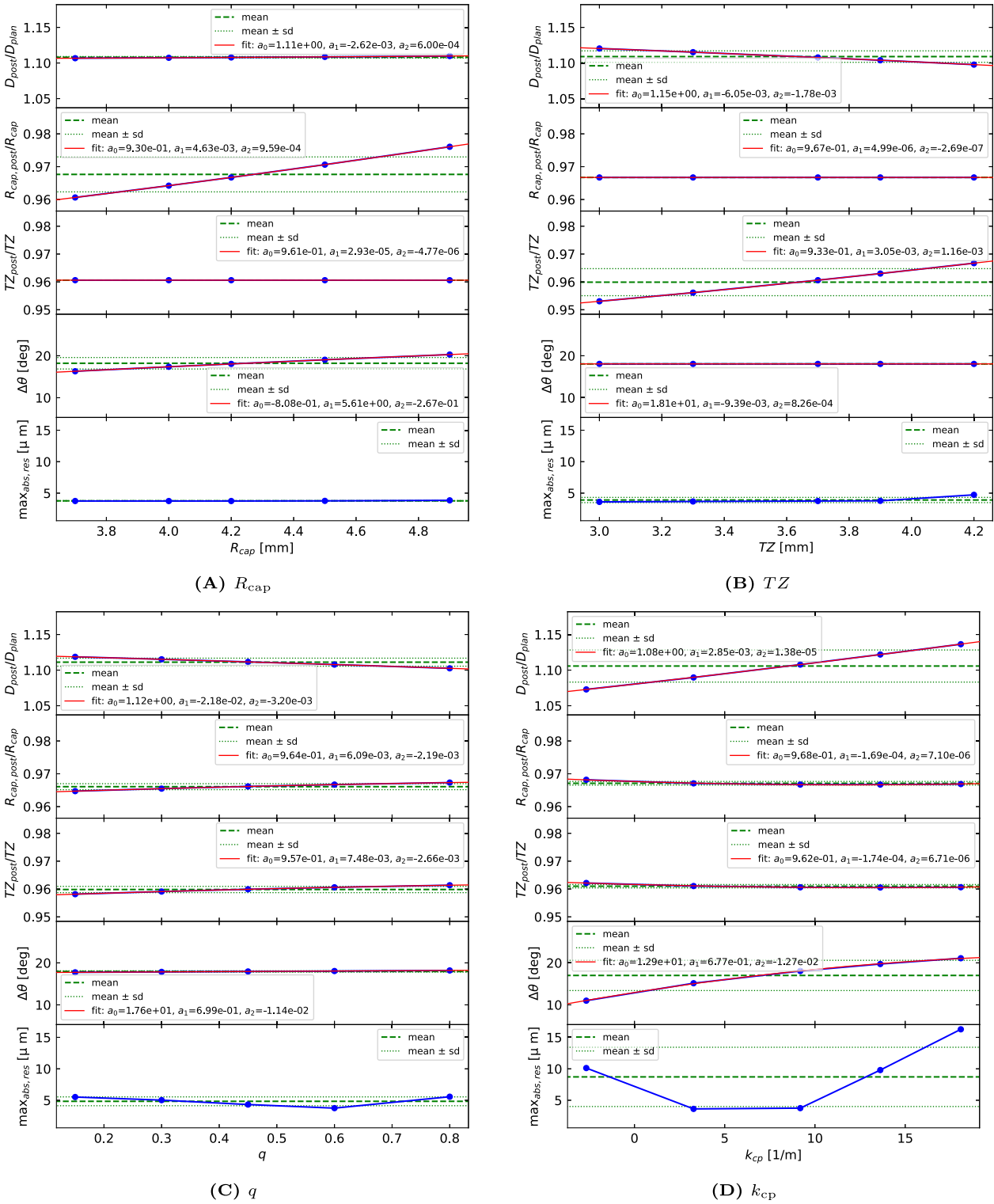


Figure 8: Extension of Figure 3. Various parameter variations for the ratio of D_{post}/D_{plan} , $R_{cap,post}/R_{cap}$ and TZ_{post}/TZ , the deviation in incision angle $\Delta\theta$ and maximal absolute fit residue $max_{abs,res}$. In order to model the ratios and the deviation in incision angle, second order polynomials $y_a(x) = a_0 + a_1x + a_2x^2$ are fitted to the five scenarios.

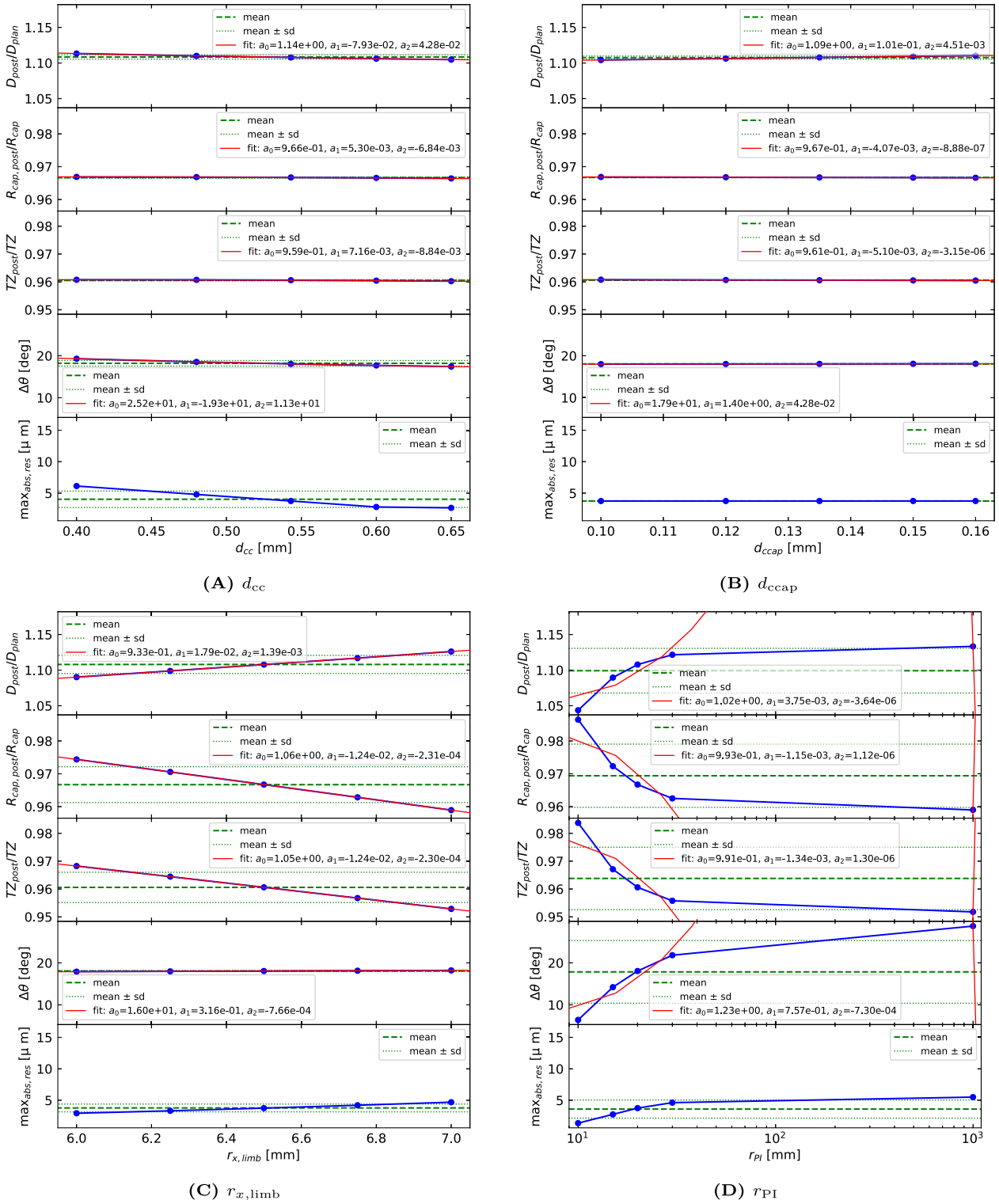


Figure 9: Extension of Figures 3 and 8. Various parameter variations for the ratio of D_{post}/D_{plan} , $R_{cap,post}/R_{cap}$ and TZ_{post}/TZ , the deviation in incision angle $\Delta\theta$ and maximal absolute fit residue $max_{abs,res}$. In order to model the ratios and the deviation in incision angle, second order polynomials $y_a(x) = a_0 + a_1x + a_2x^2$ are fitted to the five scenarios.

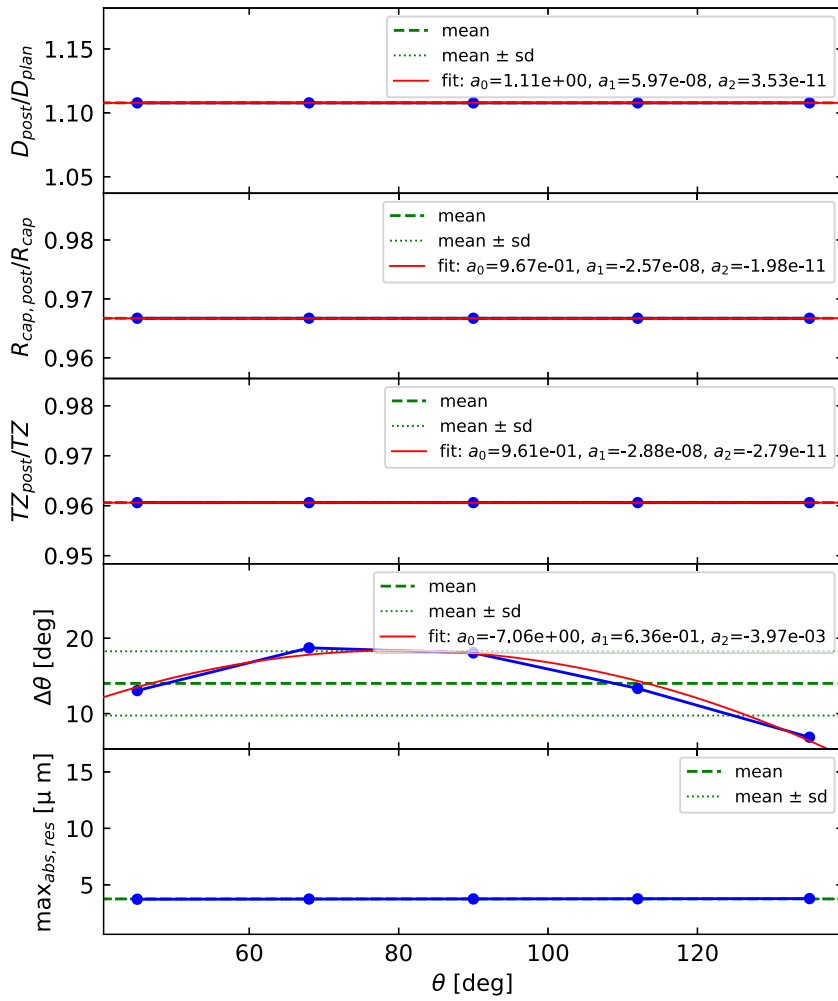


Figure 10: Extension of Figures 3, 8, and 9. Variation of θ for the ratio of D_{post}/D_{plan} , $R_{cap,post}/R_{cap}$ and TZ_{post}/TZ , the deviation in incision angle $\Delta\theta$ and maximal absolute fit residue $max_{x_{abs,res}}$. In order to model the ratios and the deviation in incision angle, second order polynomials $y_a(x) = a_0 + a_1x + a_2x^2$ are fitted to the five scenarios.

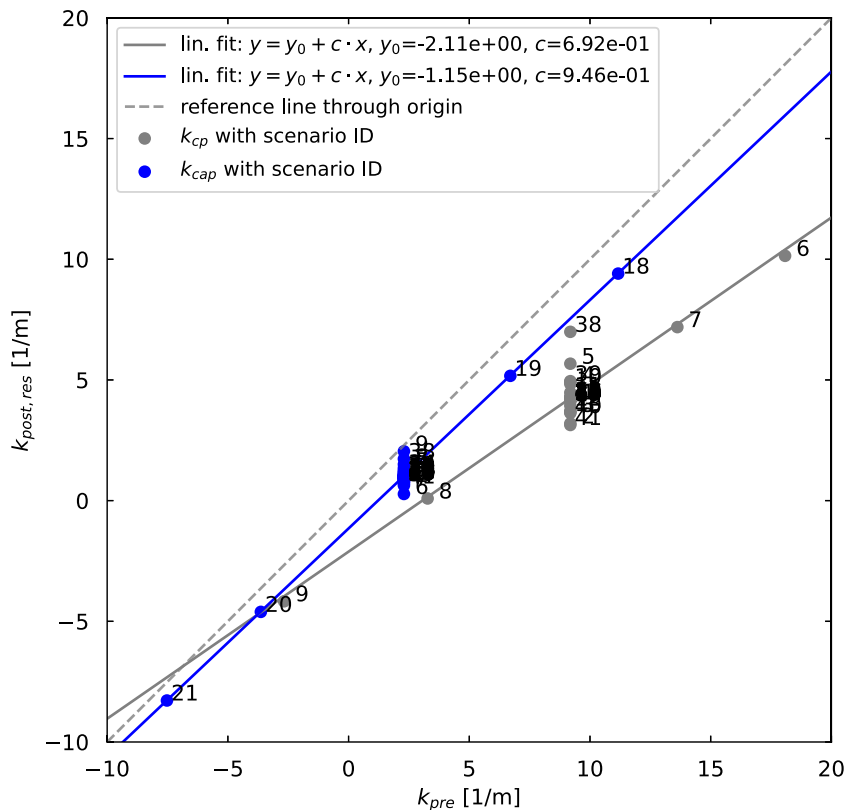


Figure 11: Comparison between pre and post rescaling values of k_{cp} and k_{cap} .

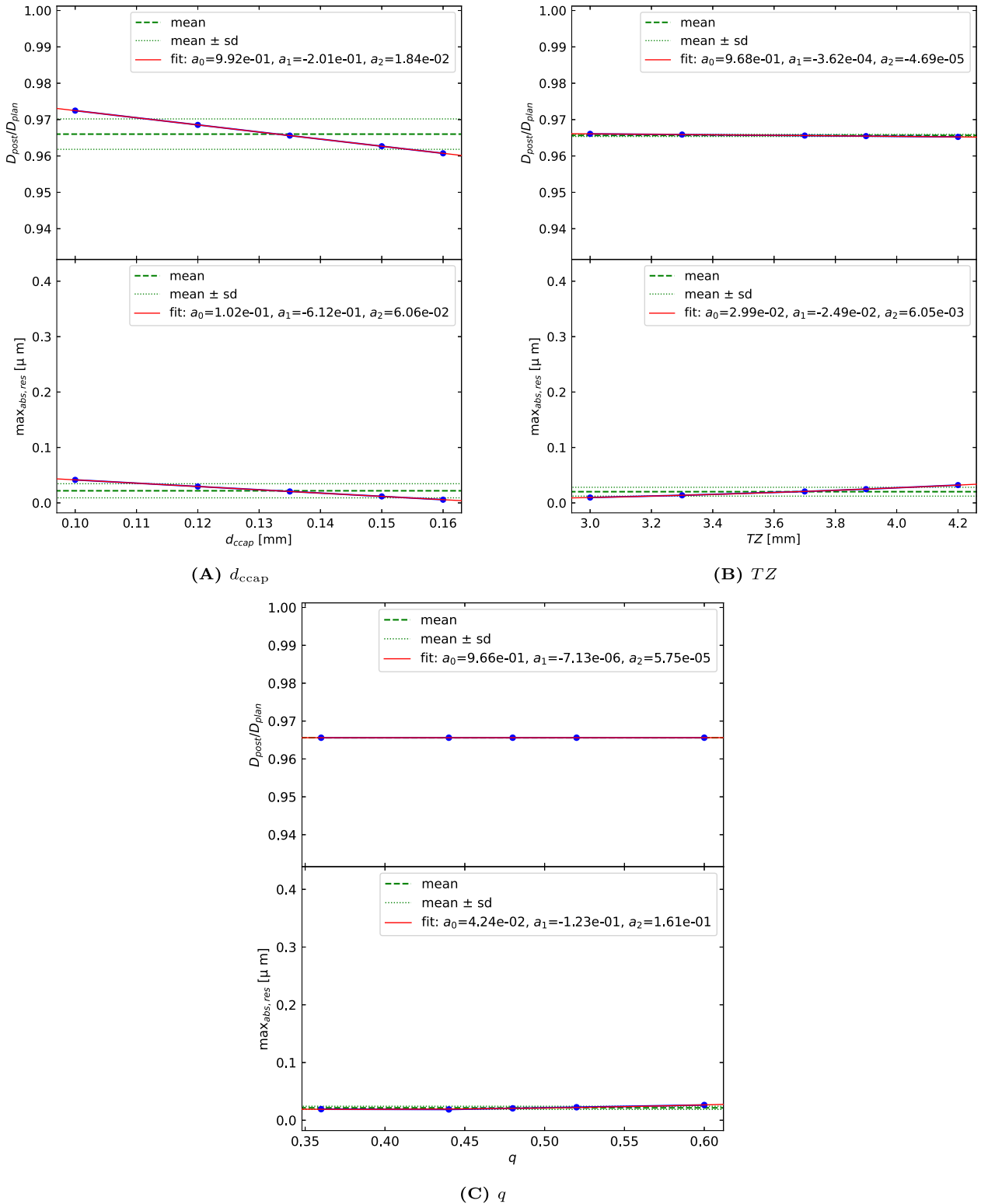


Figure 12: Closing lenticule, Section 3.2. Various parameter variations for the ratio of D_{post}/D_{plan} and maximal absolute fit residue $max_{abs, res}$. In order to model the ratio, second order polynomials $y_a(x) = a_0 + a_1x + a_2x^2$ are fitted to the five scenarios.

References

- [1] W. Sekundo, K. S. Kunert, and M. Blum, “Small incision corneal refractive surgery using the small incision lenticule extraction (SMILE) procedure for the correction of myopia and myopic astigmatism: results of a 6 month prospective study,” *Br. J. Ophthalmol.*, vol. 95, no. 3, pp. 335–339, 2010.
- [2] S. Brar, S. Ganesh, and R. R. Arra, “Refractive lenticule extraction small incision lenticule extraction: a new refractive surgery paradigm,” *Indian J. Ophthalmol.*, vol. 66, no. 1, p. 10, 2018.
- [3] R. P. Kishore and S. A. Mosquera, “Initial experience with the SCHWIND ATOS and SmartSight lenticule extraction,” *J. Clin. Res. Med.*, vol. 3, no. 4, 2020, <https://doi.org/10.31038/jcrm.2020343>.
- [4] A.-M. Samuel, P. Naubereit, S. Sobutas, et al., “Analytical optimization of the cutting efficiency for generic cavitation bubbles,” *Biomed. Opt. Express*, vol. 12, no. 7, p. 3819, 2021.
- [5] J. S. Mehta and M. Fuest, “Advances in refractive corneal lenticule extraction,” *Taiwan J. Ophthalmol.*, vol. 11, no. 2, p. 113, 2021.
- [6] R. P. Kishore and S. Arba-Mosquera, “Three-month outcomes of myopic astigmatism correction with small incision guided human cornea treatment,” *J. Refract. Surg.*, vol. 37, no. 5, pp. 304–311, 2021.
- [7] L. Izquierdo Jr., S. Daniel, O. Ben-Shaul, et al., “Corneal lenticule extraction assisted by a low-energy femtosecond laser,” *J. Cataract Refract. Surg.*, vol. 46, no. 9, pp. 1217–1221, 2020.
- [8] M. Wang, F. Zhang, C. C. Copruz, et al., “First experience in small incision lenticule extraction with the Femto LDV Z8 and lenticule evaluation using scanning electron microscopy,” *J. Ophthalmol.*, vol. 2020, pp. 1–8, 2020.
- [9] A. V. Doga, S. V. Kostenev, I. A. Mushkova, et al., “Results of corneal lenticule extraction for correction,” *Vestn. Oftalmol.*, vol. 136, no. 6, p. 214, 2020.
- [10] S. Arba Mosquera, D. de Ortueta, and S. Verma, “The art of nomograms,” *Eye Vis.*, vol. 5, no. 1, 2018, <https://doi.org/10.1186/s40662-018-0096-z>.
- [11] S. Arba-Mosquera, D. Y. S. Kang, M. H. A. Luger, et al., “Influence of extrinsic and intrinsic parameters on myopic correction in small incision lenticule extraction,” *J. Refract. Surg.*, vol. 35, no. 11, pp. 712–720, 2019.
- [12] I. Jun, D. S. Y. Kang, S. Arba-Mosquera, et al., “Comparison of clinical outcomes between vector planning and manifest refraction planning in SMILE for myopic astigmatism,” *J. Cataract Refract. Surg.*, vol. 46, no. 8, pp. 1149–1158, 2020.
- [13] H. P. Studer, K. R. Pradhan, D. Z. Reinstein, et al., “Biomechanical modeling of femtosecond laser keyhole endokeratophakia surgery,” *J. Refract. Surg.*, vol. 31, no. 7, pp. 480–486, 2015.
- [14] V. Vavourakis, J. H. Hipwell, and D. J. Hawkes, “An inverse finite element u/p-Formulation to predict the unloaded state of in vivo biological soft tissues,” *Ann. Biomed. Eng.*, vol. 44, no. 1, pp. 187–201, 2015.
- [15] P.-J. Shih, I. J. Wang, W. F. Cai, et al., “Biomechanical simulation of stress concentration and intraocular pressure in corneas subjected to myopic refractive surgical procedures,” *Sci. Rep.*, vol. 7, no. 1, 2017. <https://doi.org/10.1038/s41598-017-14293-0>.
- [16] B. Pajic, D. M. Aebersold, A. Eggspuehler, et al., “Biomechanical modeling of pterygium radiation surgery: a retrospective case study,” *Sensors*, vol. 17, no. 6, p. 1200, 2017.
- [17] M. Francis, P. Khamar, R. Shetty, et al., “In vivo prediction of air-puff induced corneal deformation using LASIK, SMILE, and PRK finite element simulations,” *Investig. Ophthalmol. Vis. Sci.*, vol. 59, no. 13, p. 5320, 2018.
- [18] D. Zhou, A. Ahmed, E. Ashkan, et al., “Microstructure-based numerical simulation of the mechanical behaviour of ocular tissue,” *J. R. Soc. Interface*, vol. 16, no. 154, p. 20180685, 2019.
- [19] L. Fang, W. Ma, Y. Wang, et al., “Theoretical analysis of wave-front aberrations induced from conventional laser refractive surgery in a biomechanical finite element model,” *Investig. Ophthalmol. Vis. Sci.*, vol. 61, no. 5, p. 34, 2020.
- [20] W. J. Dupps and C. J. Roberts, Eds. *Journal of Cataract and Refractive Surgery*, vol. 40, no. 6, in *Corneal Biomechanics*, 2014. Available at: <https://journals.lww.com/jcrs/toc/2014/06000>.
- [21] S. Arba-Mosquera, S. Verma, and S. T. Awwad, “Theoretical effect of coma and spherical aberrations translation on refractive error and higher order aberrations,” *Photonics*, vol. 7, no. 4, p. 116, 2020.
- [22] S. P. Timoshenko, *Course of Elasticity Theory. Part 2—Columns and Plates*, St. Petersburg, AE Collins Publishers, 1916.
- [23] L. N. Thibos, A. Bradley, and X. Hong, “A statistical model of the aberration structure of normal, wellcorrected eyes,” *Ophthalmic Physiol. Opt.*, vol. 22, no. 5, pp. 427–433, 2002.
- [24] J. J. Rozema, D. A. Atchison, and M.-J. Tassignon, “Statistical eye model for normal eyes,” *Investig. Ophthalmol. Vis. Sci.*, vol. 52, no. 7, p. 4525, 2011.
- [25] A. Elsheikh, C. Whitford, R. Hamarashid, et al., “Stress free configuration of the human eye,” *Med. Eng. Phys.*, vol. 35, no. 2, pp. 211–216, 2013.
- [26] P. Rodríguez, R. Navarro, and J. J. Rozema, “Eigencorneas: application of principal component analysis to corneal topography,” *Ophthalmic Physiol. Opt.*, vol. 34, no. 6, pp. 667–677, 2014.
- [27] J. J. Rozema, P. Rodríguez, R. Navarro, et al., “SyntEyes: a higher-order statistical eye model for healthy eyes,” *Investig. Ophthalmol. Vis. Sci.*, vol. 57, no. 2, p. 683, 2016.
- [28] J. J. Esteve-Taboada, R. Montés-Micó, and T. Ferrer-Blasco, “Schematic eye models to mimic the behavior of the accommodating human eye,” *J. Cataract Refract. Surg.*, vol. 44, no. 5, pp. 627–641, 2018.
- [29] R. Navarro, J. J. Rozema, M. H. Emamian, et al., “Average biometry of the cornea in a large population of Iranian school children,” *J. Opt. Soc. Am. A*, vol. 36, no. 4, p. B85, 2019.
- [30] J. H. Talamo, P. Gooding, D. Angeley, et al., “Optical patient interface in femtosecond laser-assisted cataract surgery: contact corneal applanation versus liquid immersion,” *J. Cataract Refract. Surg.*, vol. 39, no. 4, pp. 501–510, 2013.
- [31] S. Taneri, S. Arba-Mosquera, A. Rost, et al., “Results of thin-cap small-incision lenticule extraction,” *J. Cataract Refract. Surg.*, vol. 47, no. 4, pp. 439–444, 2021.